Acoustic lattice Boltzmann model for immiscible binary fluids with a species-dependent impedance

J. M. Buick

Physics and Electronics, The University of New England, Armidale, NSW 2351, Australia

J. A. Cosgrove* and R. Higham

School of Physics, The University of Edinburgh, Kings Buildings, Edinburgh EH9 3JZ, Scotland, Great Britain

A lattice Boltzmann model is considered for immiscible binary fluids with species-dependent acoustic impedance. Acoustic waves and pulses are simulated within the model, and the reflection and transmission components at the fluid interface are found to compare well with theory. The model is then applied to simulate the acoustic field due to plane-wave propagation through a bubble.

I. INTRODUCTION

In this paper we consider the propagation of an acoustic wave or pulse in an immiscible binary fluid in which the speed of sound is different for each component. Aside from purely theoretical interests this phenomenon has a large number of applications, ranging from medical to industrial. Examples include foetal imagining, diagnosing and repairing muscle damage, removing gas from a fluid by cavitation, reducing damage to propeller heads caused by high-speed bubbles, and focusing of acoustic beams in, for example, lithotriptors. The simulations are performed using the lattice Boltzmann model (LBM) [1]. The LBM has been developed as a technique for simulating fluid flow and has proved to be particularly advantageous for simulating binary-fluid mixtures [2–6]. It has also been shown that the LBM can be applied to simulate acoustic waves [7–9] and the interaction between acoustic and velocity fields [10–14]. The LBM simulates the acoustic and flow phenomenon within the same model and so does not require the coupling of two distinct models. The LBM for acoustic waves applied in this paper is capable of simulation nonlinear waves with Mach number up to around 0.02. Higher Mach numbers can be achieved using a finite-difference lattice Boltzmann scheme (see, for example, [15,16]. The approach presented here could be implemented in such a model.

II. NUMERICAL MODEL

The binary fluid model applied here was originally developed by [2,3]. The fluid system evolves on a regular two-dimensional, hexagonal grid with six links $i=1,\ldots,6$, joining each site to its six nearest neighbors. A rest link $i=0$ is also defined. The fluid is described in terms of two distribution functions: f_i representing the combined fluid and Δ_i representing the order parameter of the binary system. The combined fluid density ρ, the fluid velocity $\boldsymbol{u}$, and the order parameter $\Delta\rho$ are found from these distribution functions as

$$\rho = \sum_i f_i \quad \rho\boldsymbol{u} = \sum_i f_i\rho\boldsymbol{u}, \quad \Delta\rho = \sum_i \Delta_i. \tag{1}$$

The evolution of the distribution functions is determined by two lattice Boltzmann equations

$$f_i(\boldsymbol{r}+\boldsymbol{e}_i,t+\Delta t)-f_i(\boldsymbol{r},t)=-\frac{1}{\tau_\rho}(f_i-\overline{f_i}) \tag{2}$$

and

$$\Delta_i(\boldsymbol{r}+\boldsymbol{e}_i,t+\Delta t)-\Delta_i(\boldsymbol{r},t)=-\frac{1}{\tau_\Delta}(\Delta_i-\overline{\Delta_i}), \tag{3}$$

where τ_ρ and τ_Δ are independent relaxation parameters. Following [2,3], the form for the equilibrium distribution functions f_i and Δ_i is selected to describe a binary fluid consisting of two ideal gases with a repulsive interaction energy:

$$\overline{f_i}=\begin{cases} A_0 + C_0 u^2, & i=0, \\ A + Be_{i\alpha}u_\alpha + Cu^2 + Du_\alpha u_\beta e_{i\alpha}e_{i\beta} + G_{\alpha\beta}e_{i\alpha}e_{i\beta}, & i=1,2,6, \end{cases} \tag{4}$$

and

$$\overline{\Delta_i}=\begin{cases} a_0 + c_0 u^2, & i=0, \\ a + be_{i\alpha}u_\alpha + cu^2 + du_\alpha u_\beta e_{i\alpha}e_{i\beta}, & i=1,2,\ldots,6, \end{cases} \tag{5}$$

where

$$A_0 = \rho - 2\left[\rho T - \frac{\kappa}{2}(\rho\nabla^2\rho + \Delta\rho\nabla^2\Delta\rho)\right],$$

$$A = \frac{1}{3}\left[\rho T - \frac{\kappa}{2}(\rho\nabla^2\rho + \Delta\rho\nabla^2\Delta\rho)\right],$$

$$B = \rho/3,$$

$$C_0 = -\rho,$$

*Also at Professional Scientific Limited, ETTC Biospace, Kings Buildings, Edinburgh EH9 3JF, Scotland, Great Britain.

$$C = -\frac{\rho}{6},$$

$$D = \frac{2\rho}{3},$$

$$G_{xx} = -G_{yy} = \frac{\kappa}{3}\left[\left(\frac{\partial \rho}{\partial x}\right)^2 - \left(\frac{\partial \rho}{\partial y}\right)^2 + \left(\frac{\partial \Delta\rho}{\partial x}\right)^2 - \left(\frac{\partial \Delta\rho}{\partial y}\right)^2\right],$$

$$G_{xy} = \frac{2\kappa}{3}\left(\frac{\partial \rho}{\partial x}\frac{\partial \rho}{\partial y} + \frac{\partial \Delta\rho}{\partial x}\frac{\partial \Delta\rho}{\partial y}\right),$$

$$a_0 = \Delta\rho - 2\Gamma\Delta\mu,$$

$$a = \frac{\Gamma\Delta\mu}{3},$$

$$b = \frac{\Delta\rho}{3},$$

$$c_0 = -\Delta\rho,$$

$$c = -\frac{1}{6}\Delta\rho,$$

$$d = \frac{2}{3}\Delta\rho. \tag{6}$$

Here Γ is the mobility, $\Delta\mu$ is the chemical-potential difference between the two components, T is the temperature, κ is the interfacial energy, and Λ measures the strength of the interaction. This binary-fluid model can be shown to satisfy the Navier-Stokes equation [3]

$$\partial_t \rho u_\alpha + \partial_\beta \rho u_\alpha u_\beta = -\partial_\alpha p_0 + \nu \partial_\beta \partial_\beta \rho u_\alpha + \partial_\alpha \zeta \partial_\beta \rho u_\beta \tag{7}$$

and the convection-diffusion equation

$$\partial_t \Delta\rho + \partial_\alpha \Delta\rho u_\alpha = \Gamma\theta \partial_\beta \partial_\beta \Delta\mu - \theta \partial_\alpha \left(\frac{\Delta\rho}{\rho}\partial_\beta P_{\alpha\beta}\right), \tag{8}$$

where

$$\nu = \frac{2\tau_\rho - 1}{8},$$

$$\zeta = \left(\tau_\rho - \frac{1}{2}\right)\left(\frac{1}{2} - \frac{\partial p_0}{\partial n}\right),$$

$$\theta = \left(\tau_\Delta - \frac{1}{2}\right),$$

$$\Delta\mu = -\frac{\Lambda}{2}\frac{\Delta\rho}{\rho} + \frac{T}{2}\ln\left(\frac{1 + \Delta\rho/\rho}{1 - \Delta\rho/\rho}\right) - \kappa\nabla^2\Delta\rho,$$

$$P_{\alpha\beta} = p_0\delta_{\alpha\beta} + \kappa\partial_\alpha\rho\partial_\beta\rho + \kappa\partial_\alpha\Delta\rho\partial_\beta\Delta\rho \tag{9}$$

and

$$p_0 = \rho T - \frac{\kappa}{2}(\rho\nabla^2\rho + \Delta\rho\nabla^2\Delta\rho) - \frac{\kappa}{2}(|\nabla\rho|^2 + |\nabla\Delta\rho|^2). \tag{10}$$

For $T < \Lambda/2$ the mixture separates into two immiscible phases [3].

In the LBM the density is not constrained to be constant and so acoustic waves can be simulated by introducing a density variation which will propagate at speed c_s, where the pressure term in the Navier-Stokes equation can be expressed as $p = c_s^2\rho$. This has been investigated for a single-phase fluid [7,8] for Mach numbers up to 0.02 including nonlinear acoustic phenomena. The limit on the Mach number arises from the assumption that variations in the density are negligibly small. This assumption is used in deriving the Navier-Stokes equation from the lattice Boltzmann equation.

An acoustic wave can be introduced in the same manner to the binary-fluid model described above. This gives a speed of sound $c_s = \sqrt{p_0/\rho}$. Additionally, for the binary-fluid model, introducing a density variation will perturb the terms in the equilibrium distribution functions. This will occur through the nonconstant density (as it does for a single-phase fluid) and also through the density gradient terms in Eq. (6). Consider a density (pressure) variation of amplitude $\delta\rho$ and spatial extent δr. To maintain the simulation in an approximately incompressible limit, previous work has applied the limit $\delta\rho/\rho < 0.02$. Also, in determining the Navier-Stokes equation from a Chapman-Enskog expansion it is assumed that the spatial resolution of the simulation is significantly larger than the lattice spacing—say, $\delta r > 10$. Thus, within the normal limits of the LBM, $\nabla^2\delta\rho \sim \delta\rho/(\delta r)^2 < 2 \times 10^{-4}$ and $(\nabla\rho)^2 \sim (\delta\rho)/(\delta r)^2 < 4 \times 10^{-6}$ for $\rho \simeq 1$. These terms are negligible compared to the dominant terms in Eq. (6), in particular the gradients of $\Delta\rho$ at the interface. Also, from Eq. (10), $p_0 \simeq \rho T$ away from the interface, giving $c_s \simeq \sqrt{T}$.

Further, the speed of sound can be varied by introducing a forcing term dependent on the density gradient [17]. This is introduced by modifying the lattice Boltzmann equation to

$$f_i(\mathbf{r} + \mathbf{e}_i, t + \Delta t) - f_i(\mathbf{r}, t) = -\frac{1}{\tau_\rho}(f_i - \bar{f}_i) + \frac{1}{3}\beta\boldsymbol{\nabla}\rho \cdot \mathbf{e}_i \tag{11}$$

which gives a modified speed of sound, $c_e = \sqrt{(c_s^2 - \beta)}$. Good agreement has been found with theory for the D2Q9 model (which has $c_s^2 = 1/3$) for $-2/3 < \beta < 1/3$. We note that the difference between the form of the force term used in Eq. (11) and [17] is due to the form of the underlying lattice (see [18]).

Here this model is extended such that the speed of sound is different in the two components of the binary fluid. This is done by replacing Eq. (2) with Eq. (11), where β is now a function of the order parameter, $\beta = \beta(\Delta\rho(\mathbf{x}, t))$, such that the speed of sound is different in the two phases. In principle any function of $\Delta\rho(\mathbf{x}, t)$ may be applied. Here

$$\beta(\mathbf{x}, t) = \begin{cases} 0, & \Delta\rho \leq 0, \\ \alpha, & \Delta\rho > 0, \end{cases} \tag{12}$$

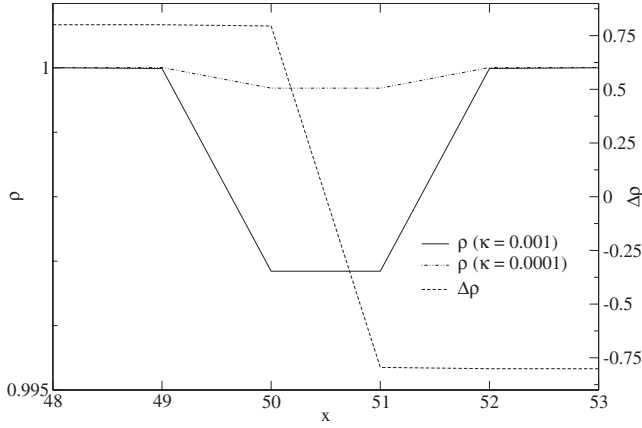is used. Assuming constant density (see Sec. III), this gives an impedance difference of

FIG. 1. Variation of the density ρ and the order parameter $\Delta\rho$ across a plane interface at $x=50.5$ for $\kappa=0.001$ and $\kappa=0.0001$.

$$\epsilon_{\Delta^-} - \epsilon_{\Delta^+} = \rho c_s (1 - \sqrt{1 - \alpha/c_s^2}) \qquad (13)$$

and a ratio of impedances

$$\frac{\epsilon_{\Delta^-}}{\epsilon_{\Delta^+}} = \left(1 - \frac{\alpha}{c_s^2}\right)^{-1/2}, \qquad (14)$$

where ϵ_{Δ^+} and ϵ_{Δ^-} are the acoustic impedances of the fluids represented by positive and negative $\Delta\rho$, respectively. The acoustic impedance for each fluid is defined explicitly in the Appendix.

III. RESULTS

In this section the propagation of acoustic signals through an immiscible binary fluid mixture, with an impedance mismatch at the fluid interface, will be considered. Acoustic pulses and waves were generated at the left boundary ($x=0$) following [17]. The distribution functions f_i were set equal to their equilibrium values, $\bar{f}_i(\rho=\rho_0+\delta\rho(t), u=0)$, where ρ_0 is the ambient density and $\delta\rho(t)$ describes the pulse or acoustic wave being implemented. Satisfactory results were obtained by neglecting the $\nabla^2\rho$ and $\nabla^2\Delta\rho$ terms. Thus $f_0(x=0, t) = (1-2T)[\rho_0 + \delta\rho(t)]$ and $f_i(x=0, t) = T[\rho_0 + \delta\rho(t)]/3$ for $i=1, 2, \ldots, 6$. The distribution functions g_i were set to $f_i\Delta\rho^\infty$, where $\Delta\rho^\infty$ is the (measured) value of $\Delta\rho$ far from the interface. At the right boundary the unknown distribution functions were determined [19] using a backward linear interpolation. Periodic boundary conditions were applied at the top and bottom boundaries.

In the following simulations the temperature, the interaction strength, and the mobility were fixed at $T=0.4$, $\Lambda=1.1$, and $\Gamma=0.1$, respectively, to simulate two immiscible fluids. Two values for the interfacial energy were used: $\kappa=0.001$ and 0.0001. The form of a plane interface is shown in Fig. 1. In both cases $\Delta\rho$ varies over one lattice unit and there is no distinguishable difference between the two values of κ. There is also a dip in the density over the interface of approximately 0.3% for $\kappa=0.001$ and 0.03% for $\kappa=0.0001$. A density difference is also present across the interface of a circular bubble. The magnitude of this difference can be determined from Laplace's equation
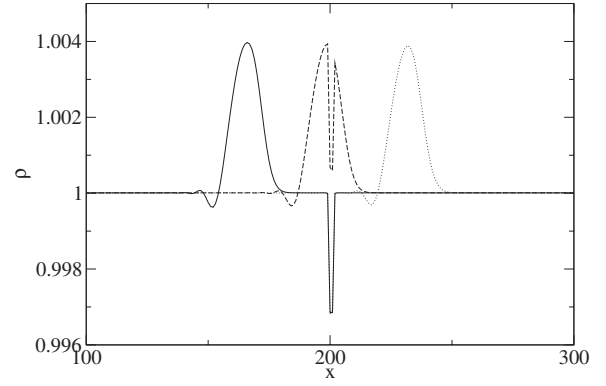

FIG. 2. An acoustic pulse propagating across the plane interface between the binary fluids with $\alpha=0$ and $\kappa=0.001$. The pulse is shown at 260 (solid line), 311 (dashed line), and 365 (dotted line) time steps.

$$\Delta p = \frac{\sigma}{r}, \qquad (15)$$

where r is the radius of the bubble, Δp is the pressure difference across the interface, and σ is the surface tension which is a function of the binary fluid parameters [4,20]. For the parameters used here this gives a negligible density difference, significantly smaller than the density dip at the interface.

The effect of the small density dip at the interface was investigated by simulating an acoustic pulse propagating perpendicular to the planar interface between two binary fluids, with no impedance mismatch ($\alpha=0$). The amplitude of the acoustic waves was selected to be comparable to the density change at the interface for $\kappa=0.001$. This is shown in Fig. 2 where the pulse is shown propagating through the interface at selected times. There was no evidence of either a reflection at the interface or a change in the amplitude of the pulse. When there is an impedance mismatch at the interface we would expect an acoustic signal to be partially transmitted and partially reflected. This is shown for the same pulse in Figs. 3 and 4 for $\alpha=-0.25$ and $\kappa=0.0001$, such that the drop
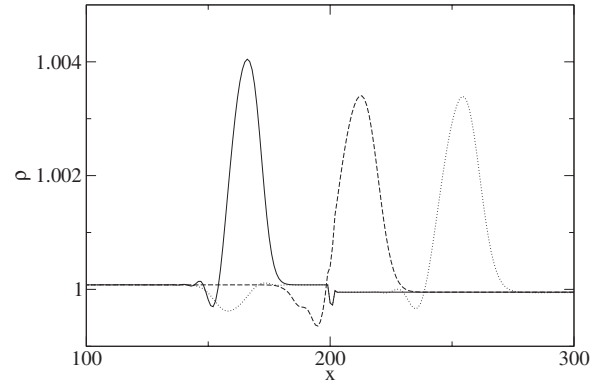

FIG. 3. An acoustic pulse propagating across the plane interface between the binary fluids with $\alpha=-0.25$ and $\kappa=0.0001$. The pulse is shown at 260 (solid line), 335 (dashed line), and 385 (dotted line) time steps.
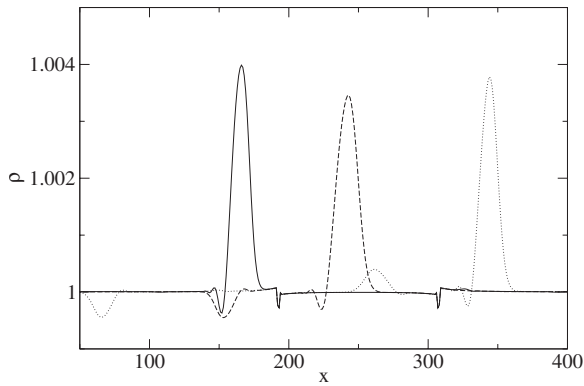
FIG. 4. An acoustic pulse propagating across a bubble with α =−0.25 and κ=0.0001. The pulse is shown at 260 (solid line), 365 (dashed line), and 505 (dotted line) time steps

in density at the interface is significantly smaller than the acoustic pulse. Figure 3 shows a plane interface between the two fluids, and Fig. 4 shows a circular bubble of fluid 2 ($\Delta\rho>0$) where the density is measured through the center of the bubble. In both cases there is clear evidence of a reflected wave at each interface and a change in the amplitude of the transmitted wave. In Fig. 4 a change in the width of the pulse is evident inside the bubble. This is expected due to the change in the speed of sound and is also evident in Fig. 3. It is also clear from Fig. 4 that any density difference between the inside and outside of the bubble, due to surface tension, is negligible for the interfacial energy applied here.

The simulation depicted in Fig. 3 was repeated for a range of α and the amplitude of the incident, transmitted, and reflected components measured. From this the transmission coefficient C_T and the reflection coefficient C_R were calculated. These are shown in Fig. 5 and compared to the theoretical expressions derived in the Appendix. Good agreement between theory and simulation is observed over the range of α.

The model was then used to investigate an acoustic wave propagating through a bubble with a higher speed of sound. The bubble was simulated with a radius of 50 lattice units and α was set to −0.4, giving a speed of sound of 0.89 inside the bubble and 0.63 outside. Plane acoustic waves were simulated moving from left to right through the fluid with a frequency of 0.1124. This gives a wavelength inside the
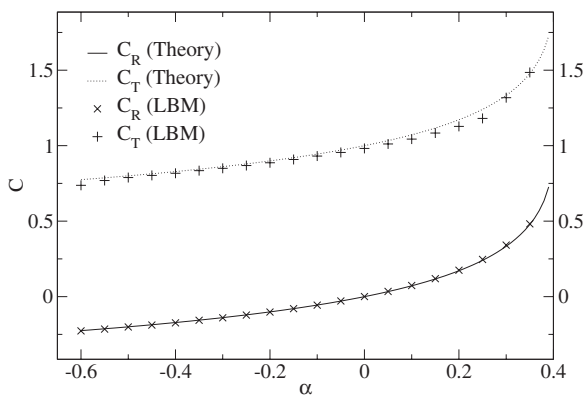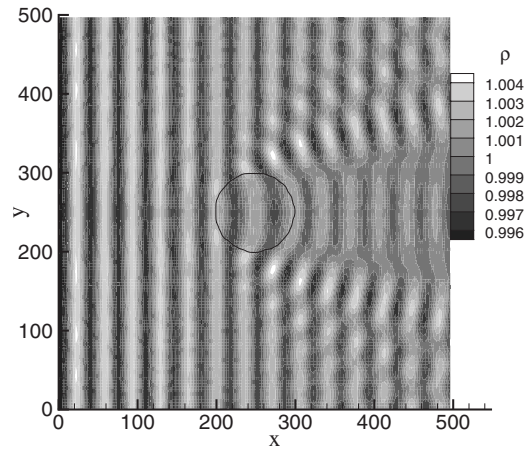

FIG. 6. The interaction between an acoustic wave and a bubble.

bubble approximately equal to the radius. The resulting density field is depicted in Fig. 6 where the position of the bubble, determined by $\Delta\rho=0$, is also shown. In front of the bubble the acoustic signal is dominated by the incident wave with a small component due to the reflected signal. Inside the bubble the transmitted component of the incident wave is also dominant; however, a reflected component from the second boundary can be observed. This can be seen in more detail in Fig. 7 which shows the density variation inside the bubble along a line through its center (y=250). The position of the wave crest and trough were recorded at every time step over a wave period and are depicted by the cross in Fig. 7 to indicate the envelope of the acoustic signal. Also shown is a sample wave which sits inside this envelope. If no reflected component was present, the envelope would show a constant value for the density (other than a small decrease with increasing x due to the viscosity of the fluid). The envelope depicted in Fig. 7 represents the steady state of the system and is independent of the period selected and the initial phase of the wave. A similar effect was observed in front of the bubble but with a smaller standing-wave component. Behind the bubble there is an interference pattern. This is due to the imaging effect of the circular bubble. Directly behind the bubble an approximately plane wave was ob-

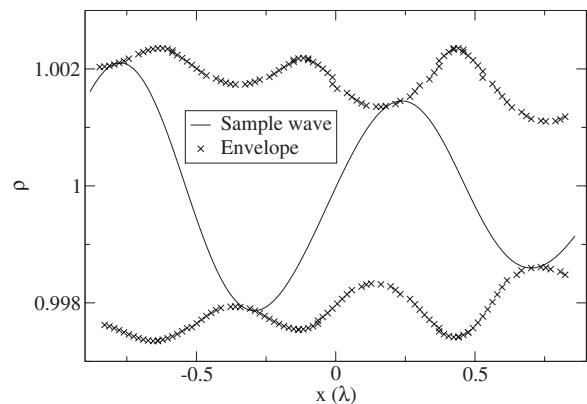FIG. 5. The reflection and transmission coefficients as a function of α.

FIG. 7. The density variation inside the bubble in Fig. 6 indicating the presence of a partial standing wave.

served to propagate away from the bubble with no standing-wave component, but with a reduced amplitude relative to the incident wave. In Fig. 7 there are a number of points where the shape of the envelope is not completely smooth—for example, the top envelope at $x=0$. These small deviations are due to the initialization of the bubble varying slightly from the final state. In particular, the system was initialized without the drop in density across the interface.

IV. CONCLUSIONS

A numerical technique based on an LBM for a binary fluid with species-dependent impedance was been investigated. Two immiscible fluids were simulated, and acoustic waves and pulses were simulated propagating across the interface. The speed of sound was varied between 0.1 and 1, and the reflection and transmission coefficients were measured. Excellent agreement was observed between the simulated coefficients and theory. The model was then applied to investigate a plane-wave propagating through a bubble with a higher speed of sound than the surrounding fluid. A partial standing wave inside the bubble and the interference pattern produced from the bubble lens were both observed.

APPENDIX: REFLECTION AND TRANSMISSION COEFFICIENTS

Consider an acoustic wave propagating from fluid 1 with speed of sound c_1 and acoustic impedance ϵ_1 to fluid 2 with speed of sound c_2 and acoustic impedance ϵ_2. At the boundary

$$\rho_i + \rho_r = \rho_t \qquad (A1)$$

and

$$u_i + u_r = u_t, \qquad (A2)$$

where the subscripts i, r, and t refer to the incident, reflected, and transmitted components, respectfully. Equations (A1) and (A2) can be expressed in terms of the pressure using $p = \rho c_s^2$ and $p = \pm \epsilon u$, where c_s is the speed of sound in the particular fluid, ϵ is the acoustic impedance, and $\pm$ refers to the direction of wave propagation. This gives

$$\frac{1}{c_1^2}(p_i + p_r) = \frac{1}{c_2^2}p_t \qquad (A3)$$

and

$$\frac{1}{\epsilon_1}(p_i - p_r) = \frac{1}{\epsilon_2}p_t. \qquad (A4)$$

Combining Eqs. (A3) and (A4) and noting that since $\rho_1 = \rho_2 = \rho$ we can express $\epsilon_1 = \rho c_1$ and $\epsilon_2 = \rho c_2$ gives

$$C_R = \frac{p_r}{p_i} = \frac{c_1 - c_2}{c_1 + c_2} \qquad (A5)$$

and

$$C_T = 1 + C_R = \frac{2c_1}{c_1 + c_2}. \qquad (A6)$$

When fluid 1 corresponds to $\beta = 0$ and fluid 2 corresponds to $\beta = \alpha$ this gives

$$C_R = \frac{c_s - \sqrt{c_s^2 - \beta}}{c_s + \sqrt{c_s^2 - \beta}} = \frac{c_s^2}{\alpha}(1 - \sqrt{1 - \alpha/c_s^2}) \qquad (A7)$$

and

$$C_T = \frac{2c_s}{c_s + \sqrt{c_s^2 - \alpha}} = \frac{2}{(1 + \sqrt{1 - \alpha/c_s^2})}. \qquad (A8)$$

[1] S. Chen and G. D. Doolen, Annu. Rev. Fluid Mech. **30**, 329 (1998).

[2] M. R. S. E. Orlandini and J. M. Yeomans, Europhys. Lett. **32**, 463 (1995).

[3] M. R. Swift, E. Orlandini, W. R. Osborn, and J. M. Yeomans, Phys. Rev. E **54**, 5041 (1996).

[4] J. M. Buick and C. A. Greated, Phys. Fluids **10**, 1490 (1998).

[5] V. M. Kendon, M. E. Cates, I. Pagonabarraga, J.-C. Desplat, and P. Bladon, J. Fluid Mech. **440**, 147 (2001).

[6] M. E. Cates, J. Vollmer, A. Wagner, and D. Vollmer, Philos. Trans. R. Soc. London, Ser. A **361**, 793 (2003).

[7] J. M. Buick, C. A. Greated, and D. M. Campbell, Europhys. Lett. **43**, 235 (1998).

[8] J. M. Buick, C. L. Buckley, C. A. Greated, and J. Gilbert, J. Phys. A **33**, 3917 (2000).

[9] L. Huang, Adv. Geophys. **48**, 517 (2007).

[10] A. Wilde, Comput. Fluids **35**, 986 (2006).

[11] D. Haydock and J. M. Yeomans, J. Phys. A **34**, 5201 (2001).

[12] D. Haydock and J. M. Yeomans, J. Phys. A **36**, 5683 (2003).

[13] J. A. Cosgrove, J. M. Buick, D. M. Campbell, and C. A. Greated, Ultrasonics **43**, 21 (2004).

[14] D. Haydock, J. Phys. A **38**, 3265 (2005).

[15] X. M. Li, R. C. K. Leung, and R. M. C. So, AIAA J. **44**, 78 (2006).

[16] M. Watari and M. Tsutahara, Physica A **364**, 129 (2006).

[17] J. M. Buick and J. A. Cosgrove, J. Phys. A **39**, 13807 (2006).

[18] J. M. Buick and C. A. Greated, Phys. Rev. E **61**, 5307 (2000).

[19] J. Boyd, J. Buick, J. A. Cosgrove, and P. Stansell, Phys. Med. Biol. **50**, 4783 (2005).

[20] K. Langaas and J. Yeomans, Eur. Phys. J. B **15**, 133 (2000).